High efficiency quasi 2D lead bromide perovskite solar cells using various barrier molecules

Bat-El Cohen[1], Małgorzata Wierzbowska[2], and Lioz Etgar[1]*

[1]The Hebrew University of Jerusalem, Institute of Chemistry, Casali Center for Applied Chemistry, Jerusalem, Israel

[2]Institute of Physics, Polish Academy of Sciences, Al. Lotnikó w 32/46, PL-02-668, Warsaw, Poland

*E-mail: lioz.etgar@mail.huji.ac.il

Abstract

This work reports on high power conversion efficiency (PCE) and high open circuit voltage (V_{oc}) of bromide-based quasi 2D perovskite solar cells. V_{oc} of more than 1.4V and at the same time, a PCE of 9.5% for cells with holes transport material (HTM), were displayed, whereas a V_{oc} value of 1.37V and PCE of 7.9% were achieved for HTM-free-based cells. The bromide quasi 2D perovskite were synthesized using various long organic barriers (e.g., benzyl ammonium-BA, phenylethyl ammonium-PEA, and propyl phenyl ammonium-PPA). The influence of different barriers' molecules on the quasi 2D perovskite's properties was studied using absorbance, X-ray diffraction, and scanning electron microscopy. No change was observed in the exciton binding energy as a result of changing the barrier molecule. Density functional theory (DFT) with Spin-orbit coupling calculations showed that in the case of BA, holes are delocalized over the whole molecule, whereas for PEA and PPA, they are delocalized more at the phenyl ring. This factor influences the electrical conductivity of holes, which is the highest for BA in comparison with the other barriers. In case of electrons, the energy onset for the nonzero conductivity is the lowest for BA. Both calculations support the better PV performance observed for the quasi 2D perovskite based on the BA as the barrier. Finally, using contact angle measurements, it was shown that the quasi 2D perovskite is more hydrophobic than the 3D perovskite. Stability measurements showed that cells based on quasi 2D perovskite are more stable than cells based on 3D perovskite.

Introduction

In recent years organic-inorganic halide perovskite has attracted much attention as a light absorber material for solar cell applications. The commonly used perovskite material in photovoltaic (PV) devices is a three-dimensional (3D) structural framework corresponding to the formula ABX_3. With organic-inorganic halide perovskite 'A' is an organic ammonium cation (usually MA-methyl ammonium or FA- formamidinium), 'B' is a divalent metal (usually Pb or Sn), and 'X' is a halogen (Cl, Br, or I). In the 3D perovskite structure, the organic ammonium cations' 'A' occupy the holes in the inorganic BX_6^{2-} corner-sharing octahedra. A useful tool for determining the perovskite formation and structure is the Goldschmidt's tolerance factor[1,2] $t = \frac{R_A + R_X}{\sqrt{2}(R_B + R_X)}$, where $R_A, R_B,$ and R_X are the ionic radii of the corresponding ions (assuming that the individual ions are hard spheres). The perovskite structure can be predicted using a simple geometric consideration; with 3D perovskite the value of 't' is from 0.8 to 1. A tolerance factor of $t \approx 1$ results in the formation of a cubic perovskite structure, whereas the lower t values result in a cubic structure of lower symmetry, such as tetragonal or orthorhombic.

Considering the Goldschmidt tolerance factor, the use of a small organic ammonium cation 'A' ($0.8 \leq t \leq 1$) forms a 3D perovskite structure, whereas the use of a larger organic ammonium cation 'R' ($t \geq 1$), which does not fit well inside the octahedral framework, results in two-dimensional (2D) perovskite $(R)_2BX_4$. Mixing both long and short organic ammonium cations result in an interesting class of layered quasi 2D perovskite structures in which the perovskite octahedra become separated by the long organic ammonium cations forming low-dimensional $(R)_2(A)_{n-1}B_nX_{3n+1}$. In this structure the number of perovskite layers (n) between the organic "barriers" (R) can be varied by controlling the stoichiometry of the components in the perovskite solution ($n = \infty$ represents 3D perovskites).[3] The traditional 3D perovskite exhibits superior electronic properties such as small exciton binding energy and long diffusion length among others, making them promising for PV applications. [4,5,6,7] On the other hand, 2D perovskite has electronic properties different from their 3D counterparts (such as a high exciton binding energy and a large band gap),[8,9] making it challenging to use them in PV applications.

The implantation of quasi 2D perovskite as a light-absorbing material in perovskite solar cell (PSC) was reported in 2014 by Smith et al.[10] using $(PEA)_2(MA)_2Pb_3I_{10}$

perovskite. Although the solar cell performance was poor (an efficiency of 4.7%), the authors predicted future intensive research on quasi 2D perovskite owing to its improved moisture stability. Further studies[11,12,13] on $(R-NH_3)_2MA_{n-1}PbI_{3n+1}$ quasi 2D perovskite reported an improvement in the stability of the perovskite to moisture. However, achieving higher efficiencies for quasi 2D perovskite cells comparable to 3D perovskite cells remains a challenging task. Sargent et al.[11] fabricated quasi 2D perovskite based on planar cells with high n values (n>40), exhibiting efficiency comparable to the 3D perovskite-based cells and with a better stability than the 3D perovskite. A recent study[14] reported a hot casting deposition technique that controls the quasi 2D perovskite growth direction in planar PCSs. As a result, a significant power conversion efficiency (PCE) was achieved, approaching 12.5% for $(BA)_2(MA)_3Pb_4I_{13}$ (BA= butyl ammonium). Moreover, our recent report[15] on quasi 2D perovskite, based on mesoporous cells, indicated that it concomitantly yields high efficiency and high voltage with and without hole transport material.

Bromide based PSCs can potentially be used to as a power source in high voltage applications due to the perovskite wide band gap (~2.25eV). Several studies showed high open circuit voltage, ranging from 1.15V–1.5V, achieved with the use of 3D bromide based PSCs.[16,17,18] However, having wide band gap, limiting the theoretical efficiencies can be produced from the bromide based PSC consider the iodide based ones. For the best of our knowledge the top reported efficiency for $MAPbBr_3$ perovskite based solar cells approach ~10% PCE.[19]

PSCs without the use of Hole transport material (HTM) was first reported in 2012 by Etgar et al.[21] In this structure the perovskite functions as both: light harvester and hole conducting material, due to a direct contact between the perovskite layer and the metal contact. The use of HTM free PSCs simplified cells fabrication, improve cells stability (due to the lack of the organic HTM material) and reduces production costs of the cell. HTM free PSCs currently exceeding more than 11% PCE for $MAPbI_3$ perovskite.[20,21]

This paper presents a detailed description of bromide-based quasi 2D perovskites $(R-NH_3)_2MA_{n-1}PbBr_{3n+1}$ using different 'R' barrier groups by studying their influence on the PSC performance. The barrier molecules include benzyl ammonium (BA), phenylethyl ammonium (PEA), and propylphenyl ammonium (PPA). Absorbance and X-ray diffraction were measured for the 2D perovskite (n=1) and for the quasi 2D perovskite (n=50) with various barriers. PSCs with and without HTM were fabricated, resulting in higher open circuit voltage (V_{oc}) and higher PCE compared with the 3D

perovskite structure. Theoretical calculations including DFT and Spin orbit coupling provided information on the exciton binding energy, geometrical orientation, charge density maps, band structures, and the electrical conductivity of these quasi 2D perovskites. Finally, stability and contact angle measurements show the superior resistivity of these materials to humidity than their counterparts, the 3D perovskite.

Results and discussion:

Figure 1 presents a schematic illustration of the perovskite's dimensionality, starting from one perovskite layer (n=1) to two perovskite layers (n=2) until n=∞, which indicates the 3D perovskite. The films were prepared from solution processed deposition, by dissolving a mixture of precursors in stoichiometric ratios and spin coat it on a substrate, as details in the experimental section. Since the preparation method is a solution process deposition, starting from n>4, there are mixtures of different perovskite layers in the film[34,35]; therefore, it is termed as quasi 2D perovskite. Here perovskite films corresponding to the formula $(R)_2(MA)_{n-1}Pb_nBr_{3n+1}$, where R is the organic barrier and MA is methylammonium (CH_3NH_3), were synthesized.

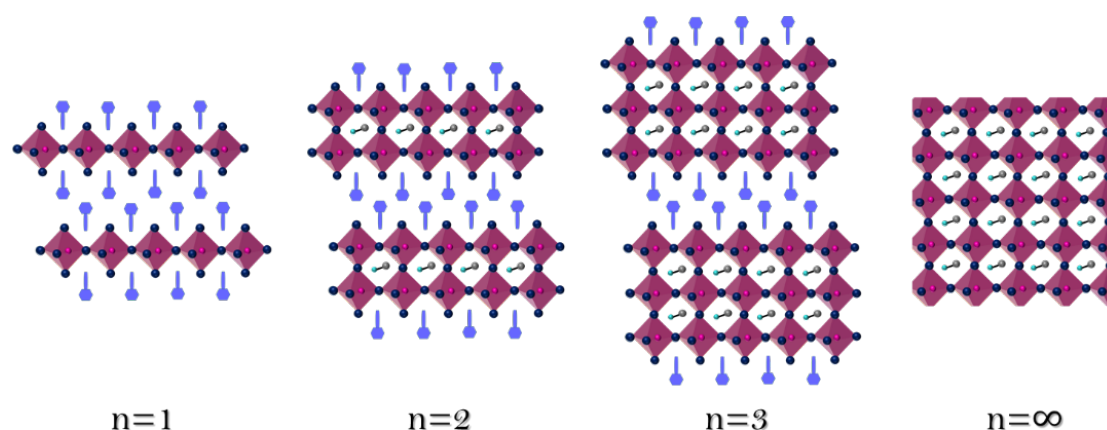$$n=1 \qquad n=2 \qquad n=3 \qquad n=\infty$$

Figure 1: Schematic illustration of hybrid halide perovskite having the structure $(R)_2(MA)_{n-1}Pb_nBr_{3n+1}$, where n=1 corresponds to 2D halide perovskite R_2PbBr_4 and n=∞ corresponds to 3D perovskite $MAPbBr_3$.

The large organic barrier 'R' was changed and the influence on the physical, crystallographic, and photovoltaic properties were investigated. The large organic barrier is responsible for forming the perovskite's dimensionality, as shown in figure 1. The studied barriers are presented in figure 2, all of which are benzene diversities that

differ in one methylene group, e.g., benzyl ammonium bromide (BABr) (figure 2A), phenyl ethyl ammonium bromide (PEABr) (figure 2B), and propyl phenyl ammonium bromide (figure 2C).
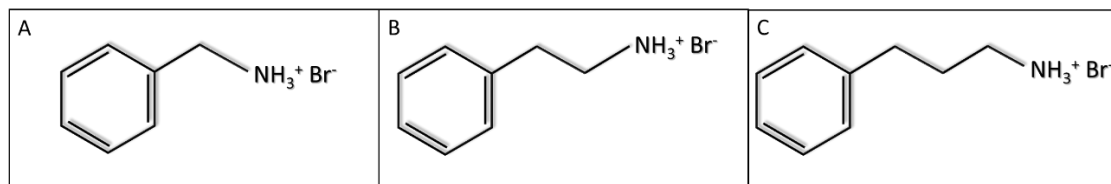

Figure 2: The chemical structure of the different barriers (R) used here have the formula $(R)_2(MA)_{n-1}Pb_nBr_{3n+1}$; (A) benzyl ammonium bromide; (B) phenylethyl ammonium bromide; and (C) propylphenyl ammonium bromide.

The 2D perovskite structure forms oriented <001> planes[22]. Figure 3A shows an X-ray diffraction (XRD) pattern of pure 2D perovskite (n=1, R_2PbBr_4) for the different barriers (e.g., BABr, PEABr and PPABr) and for the 3D perovskite (n=∞; $MAPbBr_3$). The XRD pattern for 2D perovskite exhibits highly ordered peaks, indicating the oriented c-axis of the perovskite. The absence of the peak at 2θ=15°, which corresponds to the 3D perovskite ($MAPbBr_3$) unit cell, indicates that with all the various barriers, pure 2D perovskite was formed. The XRD reflection peaks correspond to 'd' spacing in the perovskite unit cell; it can be observed that the $(BA)_2PbBr_4$ and $(PEA)_2PbBr_4$ perovskites have a similar interlayer distance of ~16.7 Å, whereas $(PPA)_2PbBr_4$ has a slightly larger interlayer distance of ~19.1 Å. The similar interlayer distance of the $(BA)_2PbBr_4$ and $(PEA)_2PbBr_4$ perovskites may be related to the conformation of the ethyl group in the organic chain.[23]

Reducing the perovskite dimensionality results in an increased bandgap due to quantum and dielectric confinement. The 2D layered perovskite has a structure with a corner-sharing MX_6^{2-} metal halide octahedra separated by large organic cations that do not fit the perovskite framework; thus, a quantum-well array is formed. In this quantum-well model the inorganic layers act as a well (forming a high dielectric constant $\varepsilon_r \approx 6$) and the organic spacer acts as a barrier ($\varepsilon_r \approx 2$).[24,25] The dielectric mismatch leads to an "image charge effect" in which the effective coulomb interaction between the electrons and holes in the well increases owing to the lower dielectric constant of the barrier.[26,27] Therefore, when the barrier is chemically changed, the exciton binding energy can be tuned.[9,25,28] In addition, the band gap energy increases for low n values due to the same

effect (described in more detail below).[9,13,15,25]   The absorbance spectra of 2D perovskite (n=1) with various barriers is presented in figure 3B. It can be clearly observed that the bandgap is increased in the 2D perovskite in comparison with the 3D perovskite. It was reported that the organic cations in high dimension halide perovskite do not have any significant contribution around the band edge,[29] therefore, no change is observed in the energy bandgap between the different barriers, as presented in figure 3B for BA, PEA, and PPA. Just a minor change is observed for the PEA barrier; this change can be related to distortion in the inorganic framework and thus, it indirectly influences the perovskite bandgap.[30]
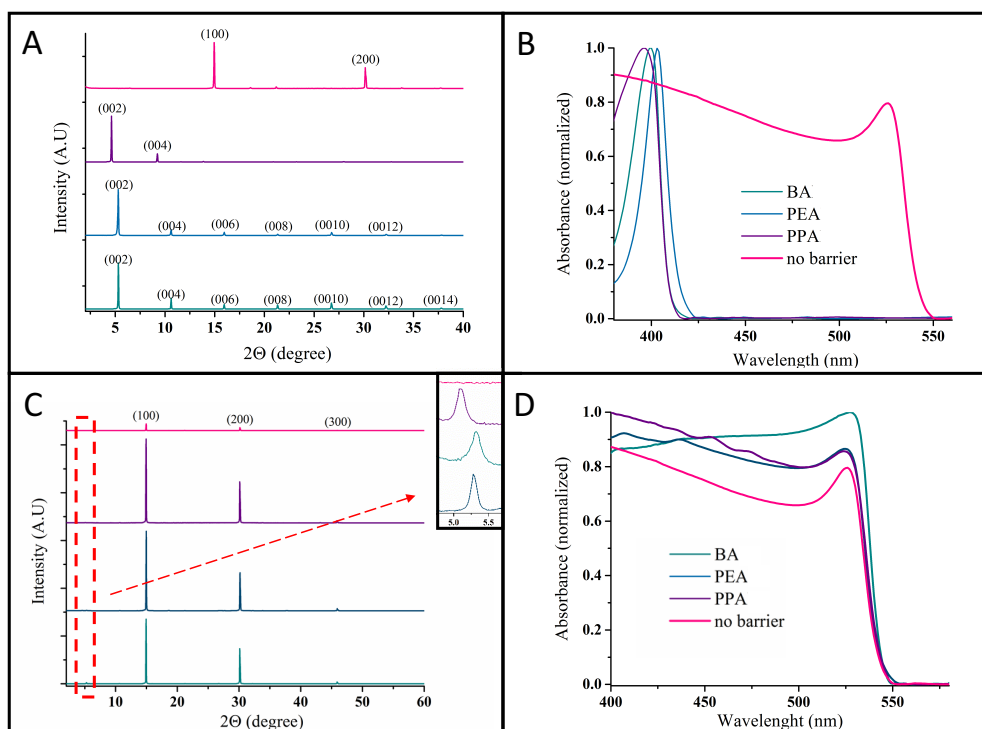

Figure 3: (A) The XRD pattern of 2D perovskite (n=1) for the different barriers, green-BABr, blue- PEABr, purple- PPABr, and pink- without a barrier (n=∞). (B) The absorbance spectra for n=1 and n=∞ for the different barriers. (C) The XRD pattern for n=50 and n=∞ for the various barriers. Inset: magnification of the peaks observed at 2θ≈ 5.2°. (D) The absorbance spectra for n=50 and n=∞ for the different barriers.

Based on our previous work[15], we were motivated to fabricate perovskite solar cells that have approximately 50 layers of perovskite as so-called quasi 2D halide perovskite. In the case of a few layers of perovskite, the transport properties are not good enough to achieve a high power conversion efficiency. Figure 3C shows the XRD pattern for n=50 layers of perovskite using the barriers BA, PEA, PPA, and MAPbBr$_3$ (the 3D

perovskite). The change in the unit cell can be detected by XRD; when a single perovskite layer is added, a reflection angle appears below $2\theta = 15°$, which is the lowest angle detected for the 3D perovskite unit cell.[31] The inset of figure 3C presents a magnification of the angle $2\theta \approx 5.2°$. It is clearly seen that a reflection peak appears in all the samples (n=50) (which are related to different barriers); however, this peak cannot be detected for the $n = \infty$ (the 3D perovskite), which supports the 2D nature of these samples. Furthermore, optical microscope images for the $R_2(MA)_{n-1}Pb_nBr_{3n+1}$ (where n=60 and R= BA/ PEA/ PPA) and 3D perovskite (n=∞) are presented in Figure 1S. The platelet nature of the layered perovskite with regard to the thick 3D crystals can be clearly detected. The absorbance spectra of n=50 layered perovskite with the different barriers is presented in Figure 3D. The band gap does not change between the different barriers; this is also related to the 3D perovskite. The exciton absorbance peak, which characterizes the bromide-based perovskite, is observed quite below the bandgap energy when n=50 (quasi 2D perovskite) and with the 3D perovskite. Additional absorbance features (related to additional excitonic states) that are assigned to the 2D and quasi 2D perovskite[8,9,13] are observed in the absorbance spectra at higher energies. In order to estimate the exciton binding energy for n=1 and n=50 for the various barriers, we used the Elliott formula, as presented in Figure 2S. [32,33] For n=1 the exciton binding energy (E_b) value was 310-320 meV for the three barriers, whereas for n=50 the E_b value was 55-56 meV for all barriers. The difference between n=1 and n=50 is clearly observed, as was previously discussed. However, no difference in the E_b value was observed between the barriers as expected.

Following the physical and optical characterizations, we introduced the quasi 2D perovskite into a solar cell structure. First, we investigated the functionality of these materials in the HTM free configuration. The quasi 2D perovskites are from the structure $(R-NH_3)_2(MA)_{n-1}Pb_nBr_{3n+1}$, where the n=40, 50, and 60 layers were investigated for the different barriers (i.e., BA, PEA, and PPA).

Figure 3S shows the cross-section HR-SEM of the HTM-free PSCs using the different barriers: BA, PEA, PPA and for 3D perovskite. In all cases the perovskite film thickness is around 400nm, whereas the TiO_2 film thickness is ca. 300nm; the gold back contact can be clearly observed having a thickness of 70nm. No change was observed between the different quasi 2D perovskites and the 3D perovskite based on the cross-section HR-SEM. However, the cubic nature of the bromide-based perovskite can be observed.

The average photovoltaic (PV) results of the different n values are presented in table 1, table 1S, and 2S for n=50, n=40, and n=60, respectively. The best average PV performance was achieved with n=50. Table 1 summarizes the average PV results and figure 10S displays the JV curves for HTM-free PSCs for quasi 2D perovskite $(R)_2(MA)_{49}Pb_{50}Br_{151,}$ (n=50), where R indicates the barrier; where for the 3D perovskite $(MAPbBr_3)$, there is no barrier.

The PV performance with BA as the barrier showed the best PV results, which were better than those of 3D perovskite. The open circuit voltage (V_{oc}) increased by 0.13V and the power conversion efficiency increased on average by 2.1%. The higher V_{oc} value observed for the quasi 2D perovskite (n=50) compared with the 3D perovskite originates from the lower radiative recombination in the layered perovskite and the lower recombination in the entire PSC.[15] With the longer barriers, namely, phenylethyl ammonium (PEA) and propylphenyl ammonium (PPA), the PV performance was lower than with the shorter barrier. (i.e., benzyl ammonium-BA) as also manifested by the decreased electrical conductivity (discussed in more detail next). However, as we reported previously[15] the PEA barrier still has higher PV performance than the 3D perovskite. The best PV performance for the HTM-free cells is shown in brackets in table 1, where a record efficiency was observed for the BA-based perovskite with 7.9% efficiency and with a V_{oc} value of 1.37V. We performed Density functional theory (DFT) calculations along with Spin-orbit coupling calculations, which showed that the electrical conductivity decreases with the length of the R group owing to the insulating character of the organic barrier.

Table 1: Average photovoltaic results for HTM-free PSCs with layered perovskite $(R)_2(MA)_{n-1}Pb_nBr_{3n+1}$ for n=50 and 3D perovskite (no barrier). In brackets are the best photovoltaic results for the corresponding conditions.

R	Voc (V)	Jsc (mA/cm^2)	FF (%)	Efficiency (%)
no barrier	1.11 ± 0.06 (1.14)	8.1 ± 0.6 (9.6)	58 ± 4 (56)	5.2 ± 0.6 (6.2)
BA	1.24 ± 0.08 (1.37)	8.9 ± 0.4 (9.0)	66 ± 2 (64)	7.3 ± 0.4 (7.9)
PEA	1.23 ± 0.02 (1.21)	8.3 ± 0.6 (9.2)	57 ± 2 (52)	5.8 ± 0.2 (5.9)
PPA	1.11 ± 0.08 (1.10)	7.6 ± 0.9 (8.8)	56 ± 3 (55)	4.7 ± 0.7 (5.5)

The optimized geometries obtained with the DFT method are presented in Figure 4SA and 4SB. The distances between the perovskite layers (Br-Br) increase from 12.1 Å to 15.4 Å in the series BA, PEA, and PPA for n=1 and from 10.6 Å to 14.8 Å for n=4 (which simulate the situation of having several dozen perovskite layers). Moreover, the NH_3 tail of BA is shifted from the C4-symmetry hollow of Br_4 to the C2-symmetry position, which enables better electronic coupling between the perovskite and the barriers (see Figure 4SB, the lower panel's left corner).

These geometrical details influence the position of the bands originating from the barriers with respect to the valence band top (VBT) and conduction band minimum (CBM). The electronic states localized at BA are the lowest of all the studied cases starting at 3.3 eV above VBT (Figure 5S color bands in the right column); this correlates well with the low energy onset of the electronic conductivity presented in Figure 4. The position of the barrier bands rise monotonically with the R-length and have a value around 4eV for PPA. This means that in order to excite the electrons into the electronic-transport active bands, high energy photons are needed while the R-length increases.

Regarding the holes, the positions of the molecular bands are deeper below VBT for BA than for PEA or PPA (Figure 5S, left column). This characteristic works in opposition to the hole-transport when the R value is short, if one thinks in terms of the activation energy needed for creating the hole, which is 1.5 eV for BA and 0.8 for PPA (Figure 5SB, left column).

However, the differential charge density maps for holes and electrons shed more light on the details of the hole delocalization at the interface of the perovskite with the barrier molecules (Figure 6S). With BA, holes are delocalized at the whole molecule, whereas for PEA and PPA, they are present more at the phenyl ring. This influences the hole's conductivity strength, which is again highest for BA in comparison with the other barriers (see the maximum of the peak for holes, which is located at -1.5 eV in Figure 4). The differential charge density maps also support the electronic conductivity picture. The electrons are delocalized over the whole BA molecule, whereas for PEA and PPA the electrons are localized along the R group. Therefore, the highest photovoltaic efficiency for BA (tables 1 and 2) agrees well with the highest carrier conductivities of BA, as shown in figure 4. It is interesting to note that both for electrons and holes the charge density is most localized for PEA (electrons from the R-group and holes at the phenyl ring) than for PPA, which correlates with the higher efficiency and higher V_{oc}

value of PEA compared with PPA. It can be concluded that when the charges are localized on the barrier molecule, a better V_{oc} can be achieved while when the charges are delocalized better current density can be achieved.
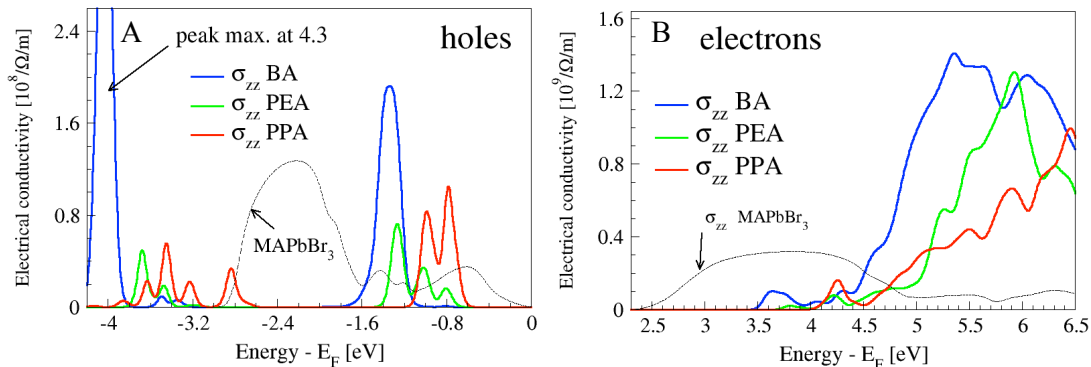

Figure 4: Electrical conductivity at 300K, plotted for holes (left) and electrons (right), for the direction across the heterostructures. The top of the valence band (Fermi level) is set at energy zero.

In addition to PSCs without HTM, we studied the quasi 2D perovskite cells with different barriers using the spiro as HTM. Table 2 summarizes the average and the best PV results. Here BA showed the best PV performance, achieving 9.5% efficiency and 11.5 mA/cm^2 current density, which approaches the Shockley & Queasier limit. The trend regarding the PV performance is the same as with HTM-free cells. The corresponding JV curves and the EQE spectra of the cells with spiro as HTM are in Figures 5B and 8SA. The shape of the EQE spectra is in good agreement with the absorbance response of the bromide quasi 2D perovskite for n=50. JV curves at different scan rates were measured for the quasi 2D and the 3D PSCs. No difference was observed in the JV curves for the various scan rates (figure 8SB), which support the stability of the PV measurements.

Furthermore, contact angle measurements were performed on the studied perovskites' surface. It was assumed that the long hydrophobic organic chain of the barrier will provide moisture resistivity to the perovskite. Previous studies of stability on perovskite with low n values showed an enhancement in resistivity to humidity.[10,11,12] Here the contact angle measurements were conducted on the n=50 samples for the various barriers. The change in the contact angle during the time of a triple distilled water (TDW) drop on the perovskite surface was measured. Figure 5C shows the change in the contact angle with time. The images of the initial drop and the drop at the final stage

can be observed in Figure 9S. As shown, the initial angle is different for the various barriers, where for 3D = 56.7°, BA=57.9°, PEA=69.1°, and PPA=69.7°. As the angle widens, the nature of the perovskite surface becomes more hydrophobic. In addition, as shown in figure 5C, PPA required the longest time to reach a low contact angle, whereas the 3D perovskite required the shortest time. It can be concluded that PPA has the most hydrophobic nature, followed by PEA, BA, and 3D perovskite. The better hydrophobic nature indicates better stability of quasi 2D perovskite in ambient air, even at high n values such as n=50.
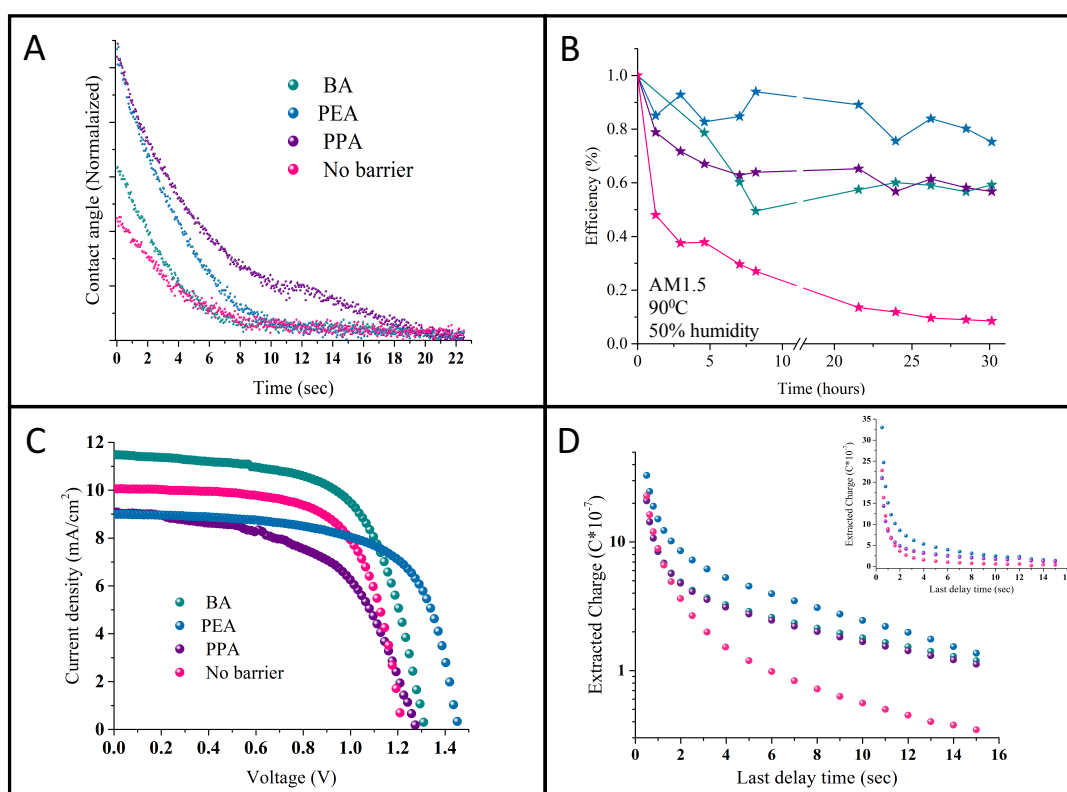

Figure 5: (A) The change in the contact angle of a drop of triple distilled water (TDW) on the studied perovskites' surface deposited on TiO_2 substrate. (B) Stability measurements of the cells using the different barrier molecules under 1 sun illumination, 90°C and 50% humidity. (C) J–V curves of the best-performing cells observed for quasi-2D (n=50) and 3D perovskite with the use of spiro as hole transport layer. (D) Charge extraction measurements for the different barriers and the 3D perovskite.

The PV performance of the cells was tracked for 60 days, where the cells were stored in nitrogen environment between measurements. The cells' PV performance didn't decrease during that time (see figure 11S). In addition, stability measurements under harsh conditions of 1 sun illumination, 90°C and 50% humidity were applied. The quasi 2D cells show enhanced stability then the 3D cells (see figure 5B). It can be observed

that the 3D cells depredated after 1 hour to half of their initial efficiency where since then their efficiency decreased to zero after 20 hours. On the other hand, the efficiency of the quasi 2D cells decreased slowly to 60% of their initial efficiency and stayed constant at this value.

Table 2: Average photovoltaic results and the best photovoltaic results (in brackets) using the hole transport layer for n=50, $(R)_2(MA)_{n-1}Pb_nBr_{3n+1}$, and for the 3D PSCs (no barrier).

R	Voc (V)	Jsc (mA/cm^2)	FF (%)	Efficiency (%)
no barrier	1.23 ± 0.05 (1.32)	9.5 ± 0.8 (10.0)	62 ± 5 (67)	7.2 ± 1.2 (8.9)
BA	1.35 ± 0.03 (1.31)	10.1 ± 0.6 (11.5)	65 ± 2 (63)	8.8 ± 0.4 (9.5)
PEA	1.45 ± 0.03 (1.45)	9.0 ± 0.3 (9.0)	59 ± 4 (65)	7.5 ± 0.6 (8.6)
PPA	1.25 ± 0.02 (1.24)	8.5 ± 0.5 (9.5)	59 ± 3 (60)	6.3 ± 0.4 (7.1)

The Hysteresis curves of quasi 2D with the different barriers and the 3D perovskite are presented in Figure 7S. The hysteresis is the largest for the longest R-group (i.e., PPA) case and smallest for the small barrier (i.e., BA) and the 3D perovskite. This is well supported by the differential charge density maps: both holes and electrons are delocalized for BA, as well as for pure MAPbBr$_3$. In addition, as discussed before, the distances between the perovskite layers (Br-Br) increase with the R group; therefore, charges are more prohibited with the PPA and PEA barriers than with BA and 3D perovskite, which results in enhanced hysteresis for PPA and PEA.

Charge extraction measurements were performed on the quasi 2D perovskite cells with the different barriers and on the 3D perovskite cell. The charge extraction method includes several steps, as we previously described. [15] Figure 5D shows the charge extracted plot vs. the delay time for the different cells. The difference between the 3D perovskite-based cell and the quasi 2D perovskite-based cells is clearly observed. With the quasi 2D-based cells, more charges are left to be extracted compared with the 3D cell. In addition, there is a slight difference between the PEA and the BA and PPA cells; however, for longer delay times this difference diminishes. As was previously reported[15], in the case of high n values (i.e. quasi 2D perovskite) more charges are

accumulated at the interface barrier/perovskite compare to low n values. Therefore, more charges are left to be extracted with the quasi 2D perovskite compared with 3D perovskite. Moreover, as stated above, based on the charge density maps, electrons and holes are localized for the PEA case than for PPA and BA, which might also explain the slight difference in the short delay time between the barriers.

Conclusions

This paper investigated the optical and physical properties of bromide quasi 2D perovskite synthesized using different barrier molecules. The various bromide quasi 2D perovskites were introduced into two PV cell configurations with and without HTM. The use of quasi 2D perovskite as an absorbent layer in PSCs yields in improved efficiencies and open circuit voltage as compared to 3D PSCs. Different barriers in the quasi 2D structures proved to affect the photovoltaic performance; the cells performance get reduced with the increasing barrier length. However, perovskite's hydrophilic character is suppressed with increase in chain length of the barrier molecule. A high open circuit voltage of 1.37V and close to 8% efficiency were observed for full bromide quasi 2D perovskite cells without HTM with BA as the barrier, and an efficiency of 9.5% (one the highest reported) was observed for the same barrier with HTM. All three barriers exhibited better PV performance and open circuit voltage than did the 3D perovskite. It was found that the energy gap and the exciton binding energy extracted using the Elliot formula does not change as a result of the barrier molecule. DFT and Spin orbit coupling calculations showed the decrease in electrical conductivity when the length of the barrier molecule is increased. Moreover, it was shown that when the charges are localized on the barrier molecule, better V_{oc} is achieved, whereas when the charges are delocalized, better current density can be achieved. Finally, contact angle and stability measurements at extreme conditions were performed. The quasi 2D perovskite showed better stability than the 3D perovskite. The contact angle measurements clearly showed the hydrophobicity nature of the quasi 2D perovskite compared with 3D perovskite.

Acknowledgments

Experimental

Perovskite precursor synthesis and solution preparation

Methylammonium bromide (MABr) was synthesized by reacting 29 mL of methylamine (40% in methanol, TCI) with 100 mL of Hydrobromic acid (48 wt% in water, Aldrich) in a 250 mL round bottom flask at 0°C for 2 hours with stirring. The solvent was removed in a rotary evaporator at 50°C for 1 hour and the precipitate was collected. This precipitate was filtered and washed with diethyl ether repeatedly three times and the white solid was collected and dried at 60 ° C in a vacuum oven for 24 hr. Benzylammonium bromide (BABr)/ phenylethylammonium bromide (PEABr)/ Propylphenylammonium bromide (PPABr) was synthesized by dropwise addition of Hydrobromic acid (48 wt% in water, Aldrich) in excess for a stirred solution of 10 ml of phenylethylammonium dissolved in 10 ml of ethanol absolute at 0°C. After the addition of acid, the precipitate was left for 20 minutes at the same temperature. The precipitate then was washed repeatedly three times with diethyl ether and recrystallized twice with ethanol absolute.

The perovskite solutions were prepared by dissolving stoichiometric quantities of components according to the molecular formula $(R)_2(MA)_{n-1}Pb_nBr_{3n+1}$ 1:1 ratio of γ-butyrolactone (GBL): Dimethyl sulfoxide (DMSO), at a 2M concentration of $PbBr_2$ (Aldrich ≥ 98%).

Device fabrication

The TiO$_2$ nanoparticles (20 nm, dyesol) were diluted in a 1:4 ratio in ethanol and spin-coated (5000 rpm, 30 sec) onto a substrate with the following architecture of SnO2:F(FTO) conductive glass (15 O cm1, Pilkington) coated by a layer of compact TiO$_2$ (TiDIP, 75% in isopropanol Aldrich). The substrate was then treated with TiCl$_4$. Perovskite solutions were dropped on the substrate and spin coated at 1000rpm for 10 seconds followed by an additional spin of 5000rpm for 60 seconds; during the second spin 40μL of toluene were dropwise added into the substrate. The films were annealed at 100°C for 1 hour.

For the HTM-fabricated cells, 40μL of 0.06M 2,2',7,7'-tetrakis-(N,N-di-4-methoxyphenylamino)-9,9'-spirofluorine (spiro-OMeTAD) in chlorobenzene with additives of 26.2 μL/1ml bis(trifl uoromethane)sulfonimide lithium salt in acetonitrile (520 mg/ml), 29.0 μL/1ml tris(2-(1 H-pyrazol-1-yl)-4- tert -butylpyridine)-cobalt(III) tri s(bis(trifl uoromethylsulfonyl)imide)) in acetonitrile (300 mg/ml), and 19.2 μL/1ml of 4- tert –butilpyridine (Aldrich) were spin coated at 4000rpm for 30 sec.

Then, 70 nm-thick gold electrode was thermally evaporated on the film under a vacuum of ~10^{-7} Torr.

Absorption measurements: Absorption measurements were performed using a Jasco V-670 spectrophotometer.

Contact angle measurement: Contact angles were collected using a Rame-Hart 100 goniometer (Rame-Hart Instrument Co., Succasunna, NJ, USA).

Photovoltaic characterization: Photovoltaic measurements were made on a New Port system, composed of an Oriel I–V test station using an Oriel Sol3A simulator. The solar simulator is class AAA for spectral performance, uniformity of irradiance, and temporal stability. The solar simulator is equipped with a 450 W xenon lamp. The output power is adjusted to match AM1.5 global sunlight (100 mW cm^2). The spectral match classi cations are IEC60904-9 2007, JIC C 8912, and ASTM E927-05. I–V curves were obtained by applying an external bias to the cell and measuring the generated photocurrent with a Keithley model 2400 digital source meter.

X-ray diffraction: X-ray diffraction measurements were performed on a D8 Advance diffractometer (Bruker AXS, Karlsruhe, Germany) with a secondary graphite monochromator, 2° Soller slits, and a 0.2 mm receiving slit. XRD patterns ranging from 2° to 75° 2q were recorded at room temperature using CuKa radiation (l= 1.5418 Å) with the following measurement conditions: a tube voltage of 40 kV, a tube current of 40 mA, a step-scan mode with a step size of 0.02˚ 2θ, and a counting time of 1 s/step.

Oriel IQE-200 was used to determine the monochromatic incident photon-electric current conversion efficiency. Under full computer control, light from a 150 W xenon arc lamp was focused through a monochromator in the 300–1800 nm wavelength range onto the photovoltaic cell being tested. The monochromator was incremented through the visible spectrum to generate the IPCE (λ), as defined by IPCE (λ) = 12 400 ($J_{sc}/\lambda\phi$), where l is the wavelength, J_{sc} is the short-circuit photocurrent density (mA cm^2), and ϕ is the incident radiative flux (mW cm^2). Photovoltaic performance was measured by using a metal mask with an aperture area of 0.04 cm^2.

Charge Extraction Measurements. Charge extraction measurements were performed using an Autolab Potentiostat-Galvenostat (PGSTAT) with a FRA32M LED driver equipped with a white light source. The cells were illuminated from the substrate side. Nova 1.11 software program was used to collect and analyze the data obtained. A typical charge extraction experiment consisted of (1) A two-second step in which the cell is discharged in the dark. (2) The cell is then disconnected and illuminated for 2 seconds (illumination time). (3) The light is then switched off and the system waits a certain time called the delay time. In this step a charge is recombined inside the cell. (4) The cell is then reconnected and the charges that were left and did not recombine are extracted and measured. This process is repeated for different delay times, ranging from 0.5 seconds to 15 seconds. The charges collected are plotted against the delay time to give insight into the life-span of the charges after a certain delay time.

References

[1] V. M. Goldschmidt, Naturwissenschaften, 1926, 14, 477–485.

[2] Z. Li, M. Yang, J.-S. Park, S.-H. Wei, J. J. Berry, and K. Zhu, Stabilizing Perovskite Structures by Tuning Tolerance Factor: Formation of Formamidinium and Cesium Lead Iodide Solid-State Alloys. Chem. Mater. 2016, 28, 284−292.

[3] J. Calabrese, N. L. Jones, R. L. Harlow, N. Herron, D. L. Thorn, and Y. Wang, Preparation and Characterization of Layered Lead Halide Compounds. J. Am. Chem. SOC 1991, 113, 2328-2330.

[4] Stranks, S. D., Eperon, G. E., Grancini, G., Menelaou, C., Alcocer, M. , Leijtens, T., Herz, L. M., Petrozza, A., and Snaith, H. J. Electron-Hole Diffusion Lengths Exceeding 1 Micrometer in an Organometal Trihalide Perovskite Absorber. Science 2013, 342, 341− 344.

[5] Xing, G., Mathews, N., Sun, S., Lim, S. S., Lam, Y. M., Gratzel, M., Mhaisalkar, S., and Sum, T. C. Long-Range Balanced Electron- and Hole-Transport Lengths in Organic-Inorganic $CH_3NH_3PbI_3$. Science 2013, 342, 344−347.

[6] Dong, Q., Fang, Y., Shao, Y., Mulligan, P., Qiu, J., Cao, L., and Huang, J. Electron-Hole Diffusion Lengths > 175 Mu M in SolutionGrown CH3NH3PbI3 Single Crystals. Science 2015, 347, 967−970.

[7] A. Miyata, A. Mitioglu, Paulina Plochocka, O. Portugall, J. Tse-Wei Wang, S. D. Stranks, H. J. Snaith, and R. J. Nicholas. Direct measurement of the exciton binding energy and effective masses for charge carriers in organic–inorganic tri-halide perovskites. Nature Physics 11, 582–587 (2015).

[8] E. A. Muljarov, S. G. Tikhodeev, N. A. Gippius, and Teruya Ishihara, Excitons in self-organized semiconductor/insulator superlattices: PbI-based perovskite compounds. Phys. Rev. B, 51, 1995.

[9] Ishihara, T. J. Lumin. 1994, 60 & 61, 269-274.

[10] I. C. Smith, E. T. Hoke, D. Solis-Ibarra, M. D. McGehee, and H. I. Karunadasa. A Layered Hybrid Perovskite Solar-Cell Absorber with Enhanced Moisture Stability. Angew. Chem. Int. Ed. 2014, 53, 11232 −11235.

[11] L. N. Quan, M. Yuan, R. Comin, O. Voznyy, E. M. Beauregard, S. Hoogland, A. Buin, A. R. Kirmani, K.i Zhao, A. Amassian, D. Ha Kim, and E. H. Sargent. Ligand-Stabilized Reduced-Dimensionality Perovskites. DOI: 10.1021/jacs.5b11740.

[12] C. C. Stoumpos, D. H. Cao, D. J. Clark, J. Young, J. M. Rondinelli, J. I. Jang, J. T. Hupp, and M. G. Kanatzidis. Ruddlesden−Popper Hybrid Lead Iodide Perovskite 2D Homologous Semiconductors. Chem. Mater. 2016, 28, 2852−2867

[13] D. H. Cao, C. C. Stoumpos, O. K. Farha, J. T. Hupp, and M. G. Kanatzidis. 2D Homologous Perovskites as Light-Absorbing Materials for Solar Cell Applications. J. Am. Chem. Soc. 2015, 137, 7843−7850.

[14] H. Tsai, W. Nie, J.-C. Blancon, C. C. Stoumpos, R. Asadpour, B. Harutyunyan, A. J. Neukirch, R. Verduzco, J. J. Crochet, S. Tretiak, L. Pedesseau8, J. Even8, M. A. Alam, G. Gupta, J. Lou, P. M. Ajayan, M. J. Bedzyk, M. G. Kanatzidis and A, D. Mohite, High-efficiency two-dimensional Ruddlesden– Popper perovskite solar cells. N AT U R E,2016, 5 3 6 , 312-317.

[15] B.E. Cohen, M. Wierzbowska, and L. Etgar. High Efficiency and High Open Circuit Voltage in Quasi 2D Perovskite Based Solar Cells, Adv. Funct. Mater. 2017, 1604733.

[16] Bing Cai, Yedi Xing, Zhou Yang, Wen-Hua Zhang and Jieshan Qiu, High performance hybrid solar cells sensitized by organolead halide perovskites, Energy Environ. Sci., 2013, 6, 1480.

[17] Eran Edri, Saar Kirmayer, David Cahen, and Gary Hodes, High Open-Circuit Voltage Solar Cells Based on Organic–Inorganic Lead Bromide Perovskite, J.Phys. Chem. Lett. 2013, 4, 897−902.

[18] Neha Arora, Simonetta Orlandi, M. Ibrahim Dar, Sadig Aghazada, Gwénolé Jacopin, Marco Cavazzini, Edoardo Mosconi, Paul Gratia, Filippo De Angelis, Gianluca Pozzi, Michael Graetzel, and Mohammad Khaja Nazeeruddin, ACS Energy Lett. 2016, 1, 107−112.

[19] Jin Hyuck Heo ,Dae Ho Song , and Sang HyukIm, Planar CH3NH3PbBr3 hybrid solar cells with 10.4% power conversion efficiency, fabricated by controlled crystallization in the spin-coating process. Adv. Mater. 2014, 26, 8179–8183.

[20] Bat-El Cohen, Sigalit Aharon, Alexander Dymshits, Lioz Etgar."Impact of Anti-Solvent Treatment on Carrier Density in Efficient Hole Conductor Free Perovskite based Solar Cells", The Journal of Physical Chemistry C,2015, DOI: 10.1021/acs.jpcc.5b10994.

[21] Shi, J.; Wei, H.; Lv, S.; Xu, X.; Wu, H.; Luo, Y.; Li, D.; Meng, Q. Control of Charge Transport in the Perovskite CH 3NH 3PbI 3 Thin Film. ChemPhysChem 2015, 16, 842 −847.

[22] K. Liang, D. B. Mitzi, and M. T. Prikas, Synthesis and Characterization of Organic-Inorganic Perovskite Thin Films Prepared Using a Versatile Two-Step Dipping Technique. Chem. Mater. 1998, 10, 403-411.

[23] B. Saparov and D. B. Mitzi. Organic−Inorganic Perovskites: Structural Versatility for Functional Materials Design. Chem. Rev. 2016, 116, 4558−4596.

[24] X. Hong, T. Ishihara, A. V. Nurmikko, Phys. Rev. B 1992, 45, 6961.

[25] T. Ishihara *, X. Hong, J. Ding and A.V. Nurmikko, Dielectric confinement effect for exciton and biexciton states in Pbla-based two-dimensional semiconductor structures. Surface Science 267 (1992) 323-326

[26] Keldysh, L. V. Coulomb Interaction in Thin Semiconductorand Semimetal Films. JETP Lett. 1979, 29, 658−661.

[27] Hanamura, E., Nagaosa, N., Kumagai, M., and Takagahara, T. Quantum Wells with Enhanced Exciton Effects and Optical Nonlinearity. Mater. Sci. Eng., B 1988, 1, 255−258.

[28] Tanaka, K., Takahashi, T., Kondo, T.,; Umebayashi, T., Asai, K., and Ema, K. Image Charge Effect on Two-Dimensional Excitons in an Inorganic-Organic Quantum-well Crystal. Phys. Rev. B: Condens. Matter Mater. Phys. 2005, 71, 045312.

[29] W.-J. Yin, T. Shi, and Y. Yan, Unusual defect physics in CH3NH3PbI3 perovskite solar cell absorber. Appl. Phys. Lett. 104, 063903 (2014).

[30] J. L. Knutson, J. D. Martiand, and D. B. Mitzi, Tuning the Band Gap in Hybrid Tin Iodide Perovskite Semiconductors Using Structural Templating. Inorganic Chemistry, 2005, 44, 13, 4699-7.

[31] J. H. Heo, D. H. Song, S. HyukIm, Adv. Mater. 2014, 26, 8179.

[32] N. Sestu, M. Cadelano, V. Sarritzu, F. Chen, D. Marongiu, R. Piras, M. Mainas, F. Quochi, M. Saba, A. Mura, and G. Bongiovanni, Absorption F-Sum Rule for the Exciton Binding Energy in Methylammonium Lead Halide Perovskites. J. Phys. Chem. Lett. 2015, 6, 4566−4572.

[33] R. Elliott, Intensity of Optical Absorption by Excitons. Phys. Rev. 1957, 108, 1384−1389.

[34] D. B. Mitzi et al., conducting tin halides with a layered organic- based perovskite structure. NATURE, 369, 467-469, 1994.

[35] Y. Takeoka, K. Asai, M. Rikukawa, and K. Sanui. Systematic Studies on Chain Lengths, Halide Species, and Well Thicknesses for Lead Halide Layered Perovskite Thin Films. Bull. Chem. Soc. Jpn. Vol. 79, No. 10, 1607–1613 (2006).